Calibrating gyrochronology using Galactic kinematics

Ruth Angus,[1,2,3] Yuxi (Lucy) Lu,[3,1] Dan Foreman-Mackey,[2] Adrian M. Price-Whelan,[2] and Jason Curtis[1]

[1]*Department of Astrophysics, American Museum of Natural History, 200 Central Park West, Manhattan, NY, USA*
[2]*Center for Computational Astrophysics, Flatiron Institute, 162 5th Avenue, Manhattan, NY, USA*
[3]*Department of Astronomy, Columbia University, Manhattan, NY, USA*

ABSTRACT

Gyrochronology, the method of inferring the age of a star from its rotation period, could be a powerful means for measuring the ages of low-mass stars in the Milky Way. However, although significant progress has recently been made in the calibration of empirical and semi-empirical gyrochronology models, the rotational evolution of K and M dwarfs is still poorly understood. This is because the ages and rotation periods of low-mass dwarfs are often difficult to measure precisely. Now however, with proper motion measurements from Gaia, Galactic kinematics can be used to calculate kinematic ages for ensembles of Milky Way disc stars. In this paper we use the Gaia positions, parallaxes and proper motions to infer the three-dimensional velocities of stars in the Kepler field. Based on their vertical velocities, we then calculate the kinematic ages of Kepler stars with measured rotation periods. Finally, we use the kinematic ages of these Kepler field stars, plus stars in open clusters, to calibrate a new fully empirical gyrochronology relation that captures the complex rotational evolution of cool dwarfs over a range of masses and ages. This gyrochronology model uses a Gaussian process to augment a power-law relation, in order to capture the time and color-dependence of rotational evolution. Using cross validation, we demonstrate that this relation predicts ages for the GKM dwarfs in our sample to within XX%. This new gyrochronology relation predicts the age of stars from their (dereddened) Gaia colors, rotation periods, and rotation period uncertainties. It applies to many but not all GKM dwarfs and we provide a full description of scenarios in which this relation should and should not be used.

Keywords: Stellar Rotation — Stellar Evolution — Stellar Activity — Stellar Magnetic Fields — Low Mass Stars — Solar Analogs — Milky Way Dynamics

1. INTRODUCTION

Main-sequence dwarfs are the most common stars in the Milky Way, and their ages could reveal the evolution of Galactic stellar populations and planetary systems. However, the ages of low-mass stars, particularly K and M dwarfs are difficult to measure because their luminosities and temperatures evolve slowly on the main sequence (see Soderblom 2010, for a review of stellar ages). Fortunately, rotation-dating, or 'gyrochronology' provides a promising means to measure precise ages for these cool dwarfs (*e.g.* Schatzman 1962; Weber & Davis 1967; Kraft 1967; Skumanich 1972; Kawaler 1988; Pinsonneault et al. 1989; Barnes 2003, 2007; Mamajek & Hillenbrand 2008; Barnes 2010; Meibom et al. 2011; Epstein & Pinsonneault 2014; Meibom et al. 2015; van Saders et al. 2016, 2018; Claytor et al. 2020). Stars with significant convective envelopes ($\lesssim 1.3$ M$_\odot$) have strong magnetic fields, generated by a Solar-type $\alpha - \Omega$ dynamo. These stars lose angular momentum over long timescales via magnetic braking (*e.g.* Schatzman 1962; Weber & Davis 1967; Kraft 1967; Skumanich 1972; Kawaler 1988; Pinsonneault et al. 1989). Stars arrive on the main sequence with a random distribution of rotation periods, ranging from around 1 to 10 days (*e.g.* Rebull et al. 2018), however observations of open clusters show that stellar rotation periods converge onto a unique sequence by around 500-700 million years (*e.g.* Irwin & Bouvier 2009; Gallet & Bouvier 2013). This sequence is often called the 'slow rotator sequence'. After stars reach the slow rotator sequence, the rotation period of a star can be determined, to first order, by its photometric color and age (*e.g.* Barnes 2003, 2007, 2010; Meibom et al. 2011, 2015).

A well-calibrated gyrochronology model that captures the time and mass-dependence of stellar angular momentum evolution could provide ages that are precise to within 20% for millions of Milky Way stars in the time-domain era (Epstein & Pinsonneault 2014; Najita et al. 2016; Angus et al. 2019; Claytor et al. 2020). However, gyrochronology

models are not yet fully calibrated, especially for K and M dwarfs, as they are limited by a lack of low-mass stars with precisely measured ages and rotation periods. For example, the oldest K dwarfs in an open cluster with measured rotation periods are those in Ruprecht 147 (2.7 Gyr) (Curtis et al. 2020). The oldest cluster M dwarfs with measured rotation periods are those in Praesepe (600-700 Myr) (Douglas et al. 2017; Rebull et al. 2017). Gyrochronology relations can therefore be considered untested for K dwarfs older than 2.7 Gyr and M dwarfs older than 600-700 Myr.

Once stars have converged to the slow rotator sequence, their rotation periods broadly follow a power law relation in time with an index of around 0.5 (Skumanich 1972). However, new Kepler/K2 rotation periods of stars in open clusters and asteroseismic stars, show that the exact value of this power law index varies as a function of mass and age (Angus et al. 2015; van Saders et al. 2016; Curtis et al. 2019; Spada & Lanzafame 2019). Two major phenomena in particular, 'weakened magnetic braking' and 'stalled braking' are both responsible for slowing the rate of magnetic braking. These two phenomena affect stars of different masses and ages and are thought to be generated by different physical processes. 'Weakened magnetic braking' was first observed in asteroseismic stars with rotation rates that appeared too rapid for their age (Angus et al. 2015). It affects the rotational evolution of G dwarfs older than around Solar age (4-5 Gyrs) and is thought to be caused by a shutting down of the magnetic dynamo when stars reach a Rossby number of around 2 (van Saders et al. 2016, 2018). [1] 'Stalled braking' is a different behavior that has been observed in the K dwarfs of at least three open clusters: NGC 752, NGC 6811, and Ruprecht 147 (Agüeros et al. 2018; Curtis et al. 2019, 2020). The K dwarfs in these clusters again appear to rotate too rapidly for their age, however in this case the underlying physical cause is thought to be the redistribution of angular momentum in the stellar interior (Spada & Lanzafame 2019).

With the discovery of weakened and stalled braking, it is clear that stars of different masses and ages spin-down at different rates. Because of the non-linear and time-variable relation between rotation period and age, the gyrochronology relations should not, if possible, be extrapolated to old ages or low masses where little calibration data exist. Instead, they should be actively calibrated for stars of all masses and ages. Our goal in this paper is to provide a new fully-empirical gyrochronology relation that captures the stalled braking behavior of old K and early M dwarfs.

Historically, gyrochronology calibration samples have mainly been comprised of stars in open clusters and stars with detectable acoustic pulsations, both of which can be precisely dated with stellar evolution models. However, to extend gyrochronology relations to older K and M dwarfs, it may be necessary to use alternative dating methods. Old open clusters are generally too distant for photometric rotation period measurements of faint M dwarfs, and asteroseismic analyses are impacted by the large magnetic activity signals and low-amplitudes of oscillations for low-mass stars. There is great promise, however, in using binaries as an alternative method for calibrating gyrochronology. For example, low-mass K and M dwarfs with a precisely dateable co-moving companion (*e.g.* a white dwarf, a subgiant, or a star with detectable acoustic oscillations) could be good calibrators. In addition, Galactic kinematics is a dating method with good potential for gyrochronology calibration. In Angus et al. (2020) we explored the kinematic properties of Kepler field stars and found that the velocity dispersion of stars increase with stellar rotation period, as expected (because both quantities increase with age). In Lu et al. (2021) we used the velocity dispersions of Kepler field stars to estimate their ages using an Age-Velocity dispersion Relation (AVR). In this paper, we use those kinematic ages for around 30,000 Kepler field stars to extend the gyrochronology relations into the old K and early M dwarf regime.

The star forming molecular gas clouds observed in the Milky Way have a low out-of-plane, or vertical, velocity (*e.g.* Stark & Brand 1989; Stark & Lee 2005; Aumer & Binney 2009; Martig et al. 2014; Aumer et al. 2016). In contrast, the vertical velocities of older stars are observed to be larger in magnitude on average (Strömberg 1946; Wielen 1977; Nordström et al. 2004; Holmberg et al. 2007, 2009; Aumer & Binney 2009; Casagrande et al. 2011; Ting & Rix 2019; Yu & Liu 2018). There are two possible explanations for this observed increase in velocity dispersion with age: either stars are born kinematically 'cool' and their orbits are heated over time via interactions with giant molecular clouds (see Sellwood 2014, for a review of secular evolution in the MW), or stars formed kinematically 'hotter' in the past (*e.g.* Bird et al. 2013). Either way, the vertical velocity dispersions of thin disk stars are observed to increase with stellar age. This behavior is codified by Age-Velocity dispersion Relations (AVRs), which typically express the relationship between age and velocity dispersion as a power law: $\sigma_v \propto t^\beta$, with free parameter, β (*e.g.* Holmberg et al. 2009; Yu & Liu 2018). These expressions can be used to infer the ages of groups of stars from their velocity dispersions.

Kinematic ages have been used to explore the evolution of cool dwarfs for over a decade. For example, West et al. (2004, 2006) found that the fraction of magnetically active M dwarfs decreases over time, by using the vertical

---

[1] Rossby number is the ratio of rotation period to convective overturn time.

distances of stars from the Galactic mid-plane as an age proxy, and West et al. (2008) used kinematic ages to calculate the expected activity lifetime for M dwarfs of different spectral types. Faherty et al. (2009) used tangential velocities to infer the ages of M, L and T dwarfs, and showed that dwarfs with lower surface gravities tended to be kinematically younger, and Kiman et al. (2019) used velocity dispersion as an age proxy to explore the evolution of Hα equivalent width (a magnetic activity indicator), in M dwarfs.

AVRs are usually calibrated in Galactocentric velocity coordinates ($v_\mathbf{x}$, $v_\mathbf{y}$, $v_\mathbf{z}$ or UVW), and these velocities can only be calculated with full 6D positional and velocity information, however most Kepler rotators do not have RV measurements[2]. In (Angus et al. 2020) we used velocity in the direction of Galactic latitude ($v_\mathbf{b}$) as a stand-in for $v_\mathbf{z}$ because, in the *Galactic* coordinate system, velocities can be calculated from 3D positions and *2D* proper motions. The Kepler field lies at low Galactic latitude, so $v_\mathbf{b}$ is a close approximation to $v_\mathbf{z}$ for Kepler stars. Although $v_\mathbf{b}$ velocity dispersion does not equal $v_\mathbf{z}$ velocity dispersion, it still increases monotonically over time and provides accurate age rankings for Kepler stars. In this paper however, we calculate or infer $v_\mathbf{z}$ for each Kepler star in our sample. For stars without RV measurements we infer *vertical* velocity, $v_\mathbf{z}$, by marginalizing over missing RVs using a hierarchical Bayesian model. These vertical velocities were used by Lu et al. (2021) to calculate velocity dispersions of groups of stars with similar properties, which they then converted into ages using an AVR (Yu & Liu 2018). In this paper, we use the kinematic ages calculated by Lu et al. (2021) to calibrate a new gyrochronology relation.

This paper is laid out as follows: in section **??** we describe the data used to calibrate our new gyrochronology model. In section 3 we describe how we calculated the kinematic ages of Kepler stars from their positions, proper motions and parallaxes (and RVs where available). In section 4 we describe the new model and how we fit it to the data. In section **??** we test our new model using cross validation and test its precision and accuracy, and in section **??** we discuss the successes and caveats of our new model.

---

[2] Although RVs for most will be released in *Gaia* DR3

2. THE DATA

In this study, we use the kinematic ages of Kepler field stars, plus stars in open clusters, to calibrate a new gyrochronology model. We used the sample of open cluster stars assembled and described in Curtis et al. (2020), which includes the Pleiades (120 Myr **?**), Praesepe (670 Myr Douglas et al. 2017, 2019), NGC 6811 (1.0 Gyr Curtis et al. 2019), NGC 6819 (2.5 Gyr Meibom et al. 2015), and Ruprecht 147 (2.7 Gyr Curtis et al. 2020). We also included the Sun as a data point in our calibration sample with the following properties: $P_{\mathrm{rot},\odot} = 26$ days, $\mathrm{Age}_\odot = 4.56$ Gyr, $G_{BP} - G_{RP\odot} = 0.82$ (**?**).

The field stars in our sample are all in the original Kepler field. This is partly because Kepler provides the largest samples of homogeneously measured rotation periods, and partly because its low Galactic latitude allows us to marginalize over missing RV measurements and precisely infer vertical velocity, $v_{\mathbf{z}}$. We combined two large rotation period catalogs constructed from original Kepler data: McQuillan et al. (2014) and Santos et al. (2019). These two studies used different techniques to measure rotation periods from Kepler light curves: autocorrelation functions and wavelets respectively. The Santos et al. (2019) study was specifically focused on cooler stars: K and M dwarfs, and includes a larger number of rotation periods for these stars. The combined catalogs provided rotation periods for a total of 38,710 stars.

We used the publicly available Kepler-Gaia DR2 crossmatched catalog[3] to combine the McQuillan et al. (2014) and Santos et al. (2019) rotation catalogs with the Gaia DR2 catalog of parallaxes, proper motions and apparent magnitudes. Reddening and extinction from dust was calculated for each star using the Bayestar dust map implemented in the `dustmaps` *Python* package (M. Green 2018), and `astropy` (Astropy Collaboration et al. 2013; Price-Whelan et al. 2018). We used Gaia DR2 photometric color, $G_{\mathrm{BP}} - G_{\mathrm{RP}}$, to estimate effective temperatures for the stars in our sample, using the calibrated relation in Curtis et al. (2020).

3705 stars in our sample had RV measurements available in Gaia DR2, with a median uncertainty of 1.88 kms^{-1}. Gaia DR2 included RVs for stars with Gaia apparent magnitudes between 4 and 13, and 3550 K $\lesssim T_{\mathrm{eff}} \lesssim$ 6900 K (Gaia Collaboration et al. 2018). We also crossmatched the McQuillan et al. (2014) sample with the 5th LAMOST data release (Cui et al. 2012; Xiang et al. 2019), adding a further 10623 RV measurements to the sample, and expanding the total number of stars with measured RVs to 14,328. The median uncertainty of the LAMOST RV measurements was 4.71 kms^{-1} and, given that the Gaia RVs were more precise, on average, than the LAMOST RVs, we adopted the Gaia value in cases where both were available. We note that the third Gaia data release will contain a large number of new RV measurements for the stars in our sample.

We removed stars with a Gaia parallax signal-to-noise ratio of less than 10, stars with negative parallaxes, and stars with a Gaia astrometric excess noise value greater than 5. After these cuts, 35,328 stars remained in our sample, of which 11,050 had RV measurements from either Gaia or LAMOST. We calculated 3D velocities for all stars with measured RVs using `astropy`, and *inferred* 3D velocities for the remaining 24,278 stars using the method described in section 3. check these numbers are consistent.
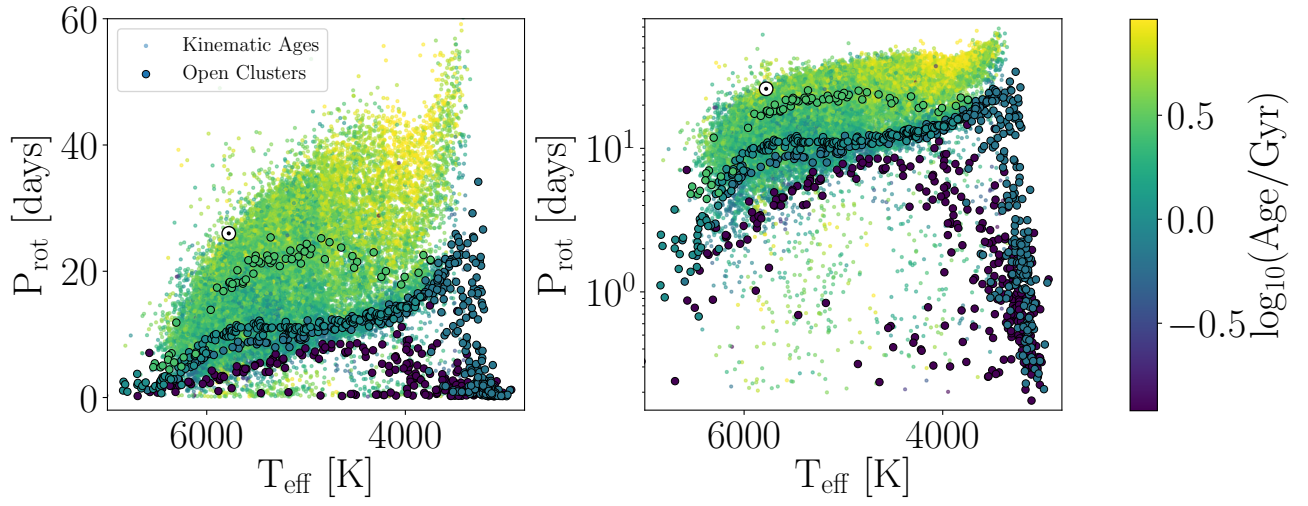
2.1. *Kinematic ages*

After calculating the vertical velocities of these stars using the method described below, we then calculated a kinematic age for each star using the method described in Lu et al. (2021). A kinematic age can be calculated from the velocity dispersion, *i.e.* standard deviation of velocities, of a group of stars. Velocity dispersion can then be converted into an age using an AVR (*e.g.* Holmberg et al. 2009; Yu & Liu 2018). In Lu et al. (2021) the kinematic ages of Kepler stars were calculated by binning them in rotation period, effective temperature, absolute Gaia magnitude and Rossby number-space. The kinematic age of each star was estimated by calculating the velocity dispersions of stars with similar parameters, and using an AVR to calculate a corresponding age. The bin size was optimized using a number of Kepler stars with asteroseismic ages. This kinematic age-dating method produced ages that were consistent with independent measurements of stellar age, for stars with available ages (stars in open clusters and asteroseismic stars, primarily). The uncertainties on these kinematic ages were estimated to be around 1-2 Gyr. Further details of this kinematic dating method are provided in that work.

Figure **??** displays the data we used to calibrate our gyrochronology model in P_{rot}-T_{eff} space. Kepler field stars are shown as small points, and cluster stars are larger points with black outlines. Points are colored by either their kinematic ages or cluster ages. The left- and right-hand panels have a linear and logarithmic y-axis, respectively.

---

[3] Available at gaia-kepler.fun

Figure 1. The calibration data. Kepler field stars are shown as small points, and cluster stars are larger points with black outlines. Points are colored by either their kinematic ages or cluster ages. The left- and right-hand panels have a linear and logarithmic y-axis, respectively.

3. STELLAR VELOCITIES

In this section we describe how we calculated full 3D velocities for the field stars in our sample, which were then used to calculate kinematic ages using the method described in Lu et al. (2021).

Most AVRs are calibrated using velocities in Galactocentric coordinates, $v_{\mathbf{x}}$, $v_{\mathbf{y}}$ and $v_{\mathbf{z}}$, which can only be calculated with full 6-D position and velocity information, i.e. proper motions, position and radial velocity. In Angus et al. (2020) we explored rotational evolution using velocity dispersion as an age proxy, however we used velocity in the direction of Galactic latitude, $v_{\mathbf{b}}$, instead of $v_{\mathbf{z}}$. This is because $v_{\mathbf{b}}$ can be calculated without an RV measurement but is a close approximation to $v_{\mathbf{z}}$ for Kepler stars due to the orientation of the Kepler field. The Kepler field lies at low Galactic latitudes, ($\sim 5 - 20°$), so the $\mathbf{z}$-direction is similar to the $\mathbf{b}$-direction for Kepler stars. However, even at such low latitudes, kinematic ages calculated with $v_{\mathbf{b}}$ instead of $v_{\mathbf{z}}$ are likely to be systematically larger because of mixing between $v_{\mathbf{z}}$, $v_{\mathbf{x}}$ and $v_{\mathbf{y}}$. A direct measurement or precise estimate of $v_{\mathbf{z}}$ is necessary to calculate accurate kinematic ages. Less than 1 in 3 stars in our sample of Kepler rotators have a directly measured RV available, and for these $\sim$11,000 stars we calculated vertical velocities, $v_{\mathbf{z}}$, using the `coordinates` library of `astropy` (Astropy Collaboration et al. 2013; Price-Whelan et al. 2018). For the remaining stars we inferred their vertical velocities by marginalizing over their RVs.

3.1. Inferring 3D velocities (marginalizing over missing RV measurements)

For each star in our sample without an RV measurement, we inferred $v_{\mathbf{x}}$, $v_{\mathbf{y}}$, and $v_{\mathbf{z}}$ from the 3D positions (right ascension, α, declination, δ, and parallax, π) and 2D proper motions (μ_α and μ_δ) provided in the Gaia DR2 catalog (Brown et al. 2011). We also simultaneously inferred distance, (instead of using inverse-parallax), to model velocities (see e.g. Bailer-Jones 2015; Bailer-Jones et al. 2018).

Using Bayes rule, the posterior probability of the velocity parameters given the Gaia data can be written:

$$p(\mathbf{v_{xyz}}, D | \mu_\alpha, \mu_\delta, \alpha, \delta, \pi) = p(\mu_\alpha, \mu_\delta, \alpha, \delta, \pi | \mathbf{v_{xyz}}, D) p(\mathbf{v_{xyz}}) p(D), \tag{1}$$

where D is distance and $\mathbf{v_{xyz}}$ is the 3D vector of velocities. To evaluate the likelihood function, our model predicted observable data from model parameters, i.e. it converted $v_{\mathbf{x}}$, $v_{\mathbf{y}}$ $v_{\mathbf{z}}$ and D to μ_α, μ_δ and π. In the first step of the model evaluation, cartesian coordinates, $\mathbf{x}$, $\mathbf{y}$, and $\mathbf{z}$ were calculated from α and δ measurements and D ($1/\pi$) for each star, by applying a series of matrix rotations, and a translation to account for the Solar position. The cartesian Galactocentric velocity parameters, $v_{\mathbf{x}}$, $v_{\mathbf{y}}$, and $v_{\mathbf{z}}$, were then converted to equatorial coordinates, μ_α and μ_δ, via another rotation.

As mentioned previously, the specific positioning of the Kepler field (at low Galactic latitude) allows $v_{\mathbf{z}}$ to be well-constrained from proper motion measurements alone. This also happens to be the case for $v_{\mathbf{x}}$, because the direction of the Kepler field is almost aligned with the $\mathbf{y}$-axis of the Galactocentric coordinate system and is almost perpendicular to both the $\mathbf{x}$ and $\mathbf{z}$-axes (see figure 2). For this reason, the $\mathbf{y}$-direction is similar to the radial direction for observers near the Sun, so $v_{\mathbf{y}}$ will be poorly constrained for Kepler stars without RV measurements. On the other hand, $v_{\mathbf{x}}$ and $v_{\mathbf{z}}$ are almost perpendicular to the radial direction and can be precisely inferred with proper motions alone.

3.2. The prior

The prior distribution over distance and velocities was constructed from the data. We calculated the means and covariances of the $v_{\mathbf{x}}$, $v_{\mathbf{y}}$, $v_{\mathbf{z}}$ and $\ln(D)$ distributions of stars with measured RVs and then used these means and covariances to construct a multivariate Gaussian prior over the parameters for stars without RVs. Velocity outliers greater than 3-σ were removed before calculating the means and covariances of the distributions. The 2-dimensional ln-distance and velocity distributions are displayed in figure 3, with 2-σ contours shown in blue.

Our goal was to infer the velocities of stars without RV measurements using a prior calculated from stars with RV measurements. However, stars with and without RVs are likely to be different populations, with parameters that depend on the Gaia and LAMOST selection functions. In particular, stars without RV measurements are more likely to be fainter, cooler, and further away. For this reason, a prior based on the velocity distributions of stars with RVs will not necessarily reflect the velocities of those without. However, given that $v_{\mathbf{x}}$ and $v_{\mathbf{z}}$ are strongly informed by proper motion measurements, and therefore likely to be relatively prior-insensitive, the prior may not impact our final vertical velocity, and subsequent kinematic ages, significantly. Remember, we are mainly interested in the $v_{\mathbf{z}}$ parameter because vertical velocity dispersion is a well-studied age indicator.

Figure 2. **x**, **y** and **z** positions of stars observed by Kepler, showing the orientation of the Kepler field. The direction of the field is almost aligned with the **y**-axis and almost perpendicular to the **x** and **z**-axes, which is why $v_\mathbf{x}$ and $v_\mathbf{z}$ can be tightly constrained for Kepler stars without RVs, but $v_\mathbf{y}$ cannot.
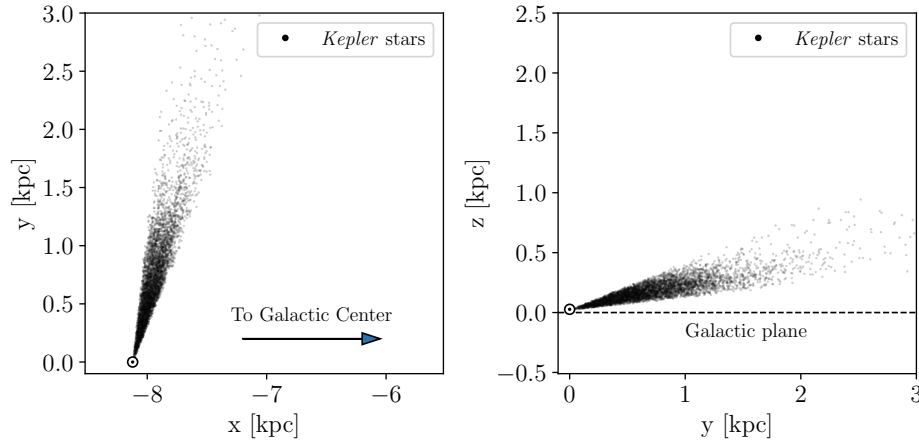
Figure 3. The 2D velocity and distance distributions for stars with RV measurements, used to construct a multivariate Gaussian prior over velocity and distance parameters for stars *without* RVs. 2-σ contours are shown in blue.
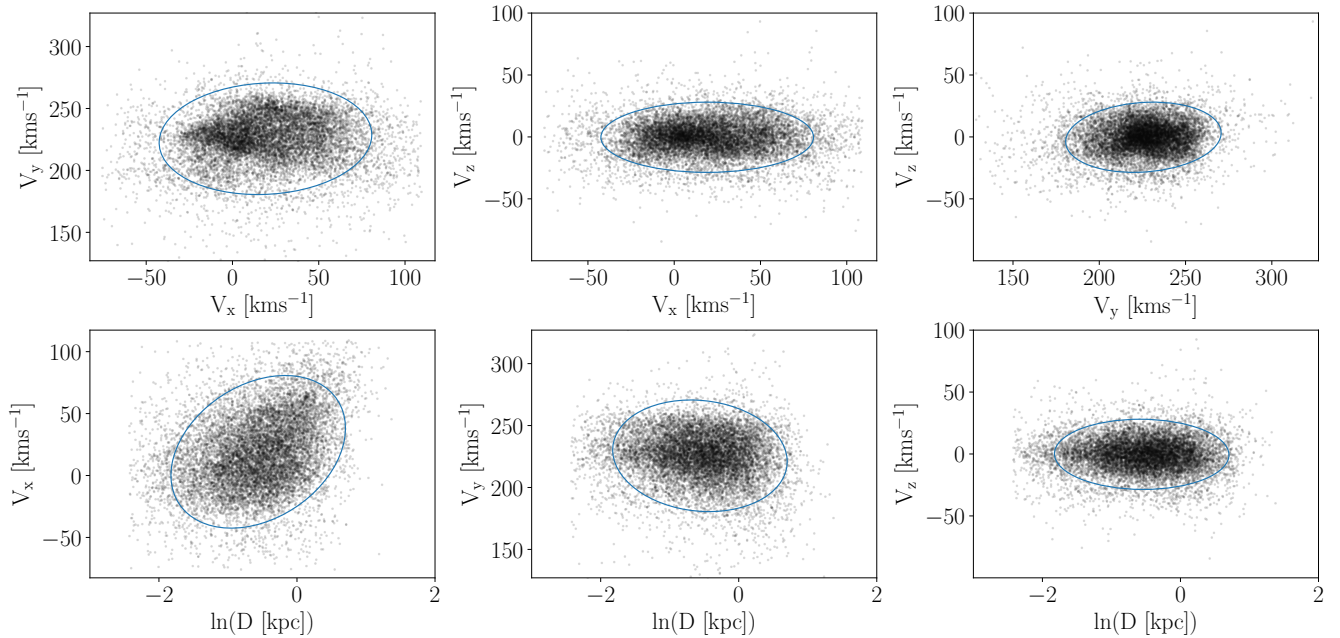
We tested the influence of the prior on the velocities we inferred. One of the main features of the *Gaia* and *LAMOST* RV selection functions is brightness: *Gaia* DR2 RVs are only available for stars brighter than around 13th magnitude, and *LAMOST* RVs for stars brighter than around 17th magnitude. Ruth, check the actual LAMOST selection function. For this reason, we tested priors based on stellar populations with different apparent magnitudes. Three priors were tested: one calculated from the velocity distributions of the brightest half of the RV sample (*Gaia G*-band apparent magnitude < 13.9), one from the faintest half ($G > 13.9$), and one from all stars with RVs. Figure 4 shows the distributions of the faint (blue) and bright (orange) halves of the RV sample as kernel density estimates (KDEs). The distributions are different because bright stars are more massive, younger, and closer to the Sun on average than faint stars. As a result, these stars occupy slightly different Galactic orbits. The Gaussian fits to these distributions, which

were used as prior PDFs, are shown in figure **??** as dashed, colored lines. The Gaussian fit to *all* the data, both bright and faint, is shown as a black solid line. The means of the faint and bright distributions differed by 6 kms^{-1}, 5 kms^{-1}, 1 kms^{-1} and 0.21 kpc, for $v_\mathbf{x}$ $v_\mathbf{y}$, $v_\mathbf{z}$ and $\ln(D)$, respectively. The $v_\mathbf{x}$, $v_\mathbf{y}$, and distance distributions of these stars are strongly dependent on brightness. However, the $v_\mathbf{z}$ distribution does not vary significantly with stellar brightness. Since $v_\mathbf{z}$ is the only velocity we actually used to infer kinematic ages, this indicates that the choice of prior does not strongly impact our final results. To confirm this, we tested the influence of the prior on the parameters.

Figure 4. Velocity and distance distributions of faint (blue) and bright (orange) stars with RVs, shown as KDEs. Gaussian fits to these distributions are shown as dashed lines in corresponding colors. The solid black line shows the Gaussian fit to all data (bright and faint combined) and is the prior we ended up using in our model.
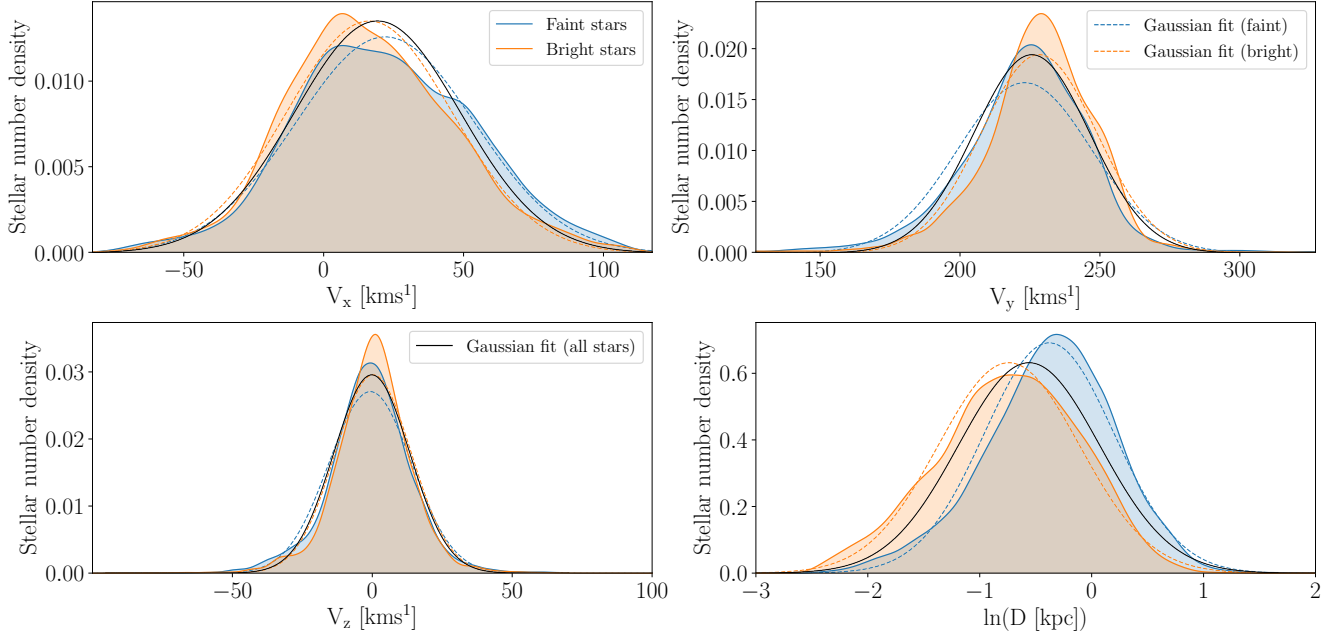
We inferred the velocities of 3000 stars chosen at random from the *Gaia-LAMOST* RV sample using each of these three priors and compared the inferred velocity distributions. If the inferred velocities were highly prior-dependent, the resulting distributions, obtained from different priors, would look very different. The results of this test are shown in figure **??**. From left to right, the three panels show the distributions of inferred $v_\mathbf{x}$, $v_\mathbf{y}$, and $v_\mathbf{z}$. The blue dashed line shows a KDE, representing the distributions of velocities inferred using the prior calculated from the faint half of the RV sample. Similarly, the solid orange line shows the distribution of inferred velocities using the prior calculated from the bright half of the RV sample, and the solid black line shows the results of the prior calculated from *all* stars with measured RVs.

The median values of the $v_\mathbf{y}$ distributions, resulting from the faint and bright priors, differ by around 4 kms^{-1}. This is similar to the difference in means of the faint and bright populations (5 kms^{-1}, as quoted above). The inferred $v_\mathbf{x}$ and $v_\mathbf{z}$ distributions differ by 2 kms^{-1} and 0.3 kms^{-1}, respectively. Regardless of the prior choice, the $v_\mathbf{x}$ and $v_\mathbf{z}$ distributions are similar because velocities in the **x** and **z**-directions are not strongly prior dependent: they are tightly constrained with proper motion measurements alone. However, the distribution of inferred $v_\mathbf{y}$ velocities *does* depend on the prior. This is because the **y**-direction is close to the radial direction for Kepler stars (see figure 2), and $v_\mathbf{y}$ cannot be tightly constrained without an RV measurement.

Although this test was performed on stars with RV measurements, which are brighter overall than the sample of stars without RVs (*e.g.* figure **??**), figure **??** nevertheless shows that $v_\mathbf{x}$ and $v_\mathbf{z}$ are not strongly prior-dependent. In this work we are only concerned with $v_\mathbf{z}$, as we only use *vertical* velocity dispersion as an age indicator. The difference in the dispersions of $v_\mathbf{z}$ velocities, calculated with the three different priors tested above was smaller than 0.5 kms^{-1}.

Figure 5. The distributions of velocity and distance parameters, inferred using three different priors. The orange line is a KDE that represents the distribution of parameters inferred with a Gaussian prior, estimated from the bright half of the RV sample ($G < 13.9$). The blue dashed line shows the results from a prior estimated from the faint half of the RV sample ($G > 13.9$. The black line shows the results from a prior calculated from all stars with RV measurements and is the prior we adopt in our final analysis.
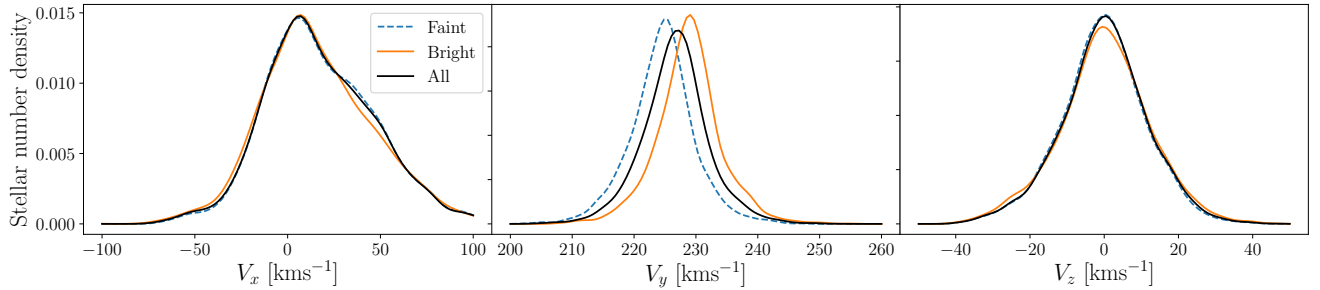
We therefore conclude that vertical velocity dispersion is relatively insensitive to prior choice, and we adopt a prior calculated from the distributions of all stars with RV measurements (black Gaussians in figure **??**).

3.3. *Inferred velocities*

For each star in the Kepler field, we explored the posteriors of the four parameters, $v_{\mathbf{x}}$, $v_{\mathbf{y}}$, $v_{\mathbf{z}}$, and $\ln(D)$ using the *PyMC3* No U-Turn Sampler (NUTS) algorithm, and the `exoplanet` *Python* library (citations). We tuned the *PyMC3* sampler for 1500 steps, with a target acceptance fraction of 0.9, then ran four chains of 1000 steps for a total of 4000 steps. Using PyMC3 made the inference procedure exceptionally fast – taking just a few seconds per star on a laptop. Check what convergence criteria you should use, or justify these choices.

To validate our method, we inferred velocities for stars in our sample with measured RVs and compared those inferred values with velocities calculated directly from 6D position, proper motion, and RV measurements. Figure **??** shows the $v_{\mathbf{x}}$, $v_{\mathbf{y}}$ and $v_{\mathbf{z}}$ velocities we inferred, for 3000 stars chosen at random, compared with those calculated from measured RVs.

The three velocity components, $v_{\mathbf{x}}$, $v_{\mathbf{y}}$ and $v_{\mathbf{z}}$ were recovered with differing levels of precision: $v_{\mathbf{x}}$ and $v_{\mathbf{z}}$ are inferred more precisely than $v_{\mathbf{y}}$. This is because of the orientation of the Kepler field, shown in figure 2. Slight inaccuracies seen in the residual panels for $v_{\mathbf{x}}$ and $v_{\mathbf{z}}$ are caused by .... Quote some summary statistics.

Figure 6. Vertical velocities calculated with full 6D information vs vertical velocities inferred without RVs, for 3000 McQuillan et al. (2014) stars with *Gaia* RV measurements.
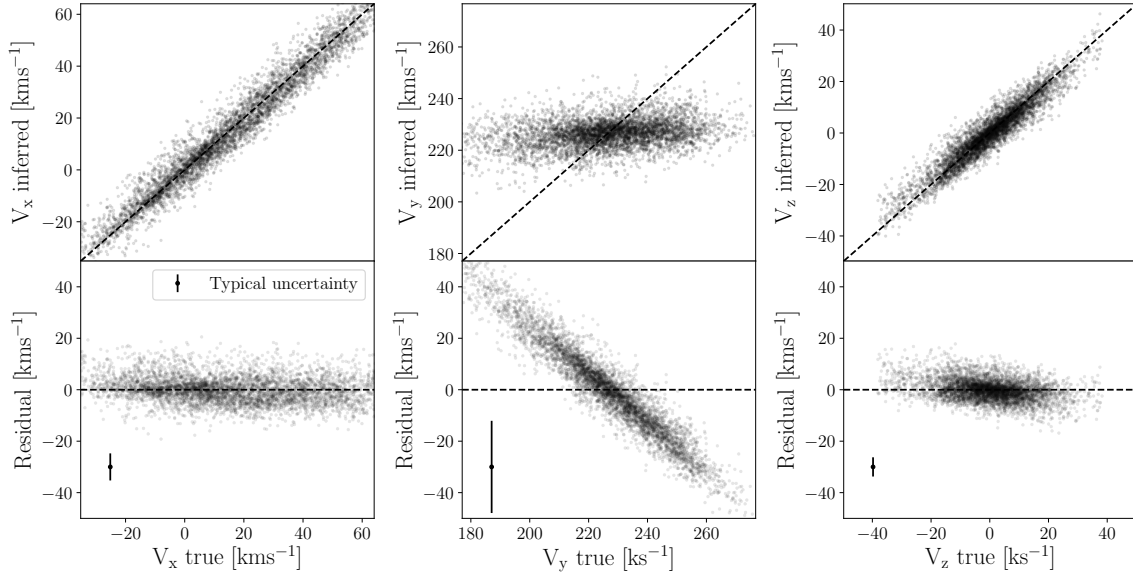
4. CALIBRATING A NEW GYROCHRONOLOGY RELATION

Using the vertical velocities of the stars in our sample, we calculated their kinematic ages using the method described in **?**. These kinematic ages, combined with the ages and rotation periods of stars in six open clusters (Pleiades, Praesepe, NGC 6811, NGC 6819, Ruprecht 147) were then used to calibrate a new gyrochronology relation via the method described below.

4.0.1. *The Model*

To calibrate a new empirical gyrochronology relation we used a composite model, consisting of an underlying mean function, augmented with a Gaussian process. The mean function is similar to previous empirical gyrochronology models and consists of two separable power-law relations: one describing the relationship between rotation period and age, and the other the relationship between rotation period and color (*e.g.* Barnes 2003, 2007; Mamajek & Hillenbrand 2008; Meibom et al. 2015; Angus et al. 2015, 2019).

Our mean function is comprised of a single power-law in age, $f(t)$, and a broken power law in color, $g(C)$:

$$P_{\text{rot}} = f(t)g(C), \tag{2}$$

where P_{rot} is rotation period in days, t is age in Gyr, and C is Gaia color, $G_{BP} - G_{RP}$. The age power-law is defined as,

$$f(t) = at^n, \tag{3}$$

following the functional form first described in Barnes (2003), where a and n are free parameters. The broken power-law in color is defined as,

$$g(C) = \left[\left(\frac{m_1}{1 + e^{s\delta}} \right) + \left(\frac{m_2}{1 + e^{-s\delta}} \right) \right]^{\delta}, \tag{4}$$

where s is a parameter that determines how smooth the break is, m_1 is the slope below (bluewards of) the power-law break, m_2 is the slope above (redwards of) the break, and

$$\delta = C - C_{\text{break}}, \tag{5}$$

where C_{break} is the color of the power-law break. In this model, s, m_1, m_2, and C_{break} are all free parameters.

We used a Gaussian process model to 'distort' this mean model, providing a better fit to the data. The GP models the residuals between the mean model and the data. We used a simple squared exponential kernel function which has only two free parameters, an amplitude, A and a length scale, l. This kernel function is defined as,

$$k_{ij} = A \exp \left[\frac{-(x_i - x_j)^2}{2l^2} \right] \tag{6}$$

4.0.2. *Fitting the model to the data*

A Gaussian process is only an appropriate model for data generated by a Gaussian process. Data with large numbers of outliers or with inaccurately estimated uncertainties are not Gaussian-distributed and therefore cannot be described with a Gaussian process. Rotation period measurements are rarely generated by a Gaussian process for two main reasons. Firstly, the uncertainties on rotation period measurements are often non-Gaussian due to aliasing and other period ambiguities. Secondly, the relationship between rotation period and color often has a large amount of intrinsic scatter. The is especially true for young stars and M dwarfs, where there is little correlation between rotation period and age. This scatter is not generated purely by measurement uncertainties which means that it cannot be described as a Gaussian process. This non-Gaussian nature of rotational data necessitated a certain amount of data formatting or 'massaging' in order to fit our model to the data. Most of these decisions could either be well-justified, or could be validated and optimized using cross validation. To obtain a good fit, we applied the following cuts to the data:

- **The cluster data**. We used a number of open clusters to calibrate our model: the Pleiades, Praesepe, the Hyades, NGC 6811, NGC 6819, and Ruprecht 147. Although the rotation periods of most G and K stars in these clusters fall on a tight sequence, the Pleiades and Praesepe contain a number of stars, particularly M dwarfs, with measured periods that are highly stochastic. Given that the scatter in M dwarf rotation periods is intrinsic: it is not produced by measurement uncertainties, these data are not well-described by a Gaussian process. For this

reason, we removed stars with stochastic rotation periods from our calibration sample. To do this, we removed all cluster stars with rotation periods shorter than one day and $G_{BP} - G_{RP} > 2.2$. We also removed cluster stars with *both* $P_{\rm rot} < 11$ days *and* $G_{BP} - G_{RP} > 1.5$. We removed all Pleaides members with $G_{BP} - G_{RP} > 1.4$. We also removed three significantly outlying G stars from the Pleiades.

- **Applying cuts to the kinematic data.** As with the cluster data, the kinematic data also needed to be Gaussian distributed. For this reason, we removed stars whose rotation periods are not determined by their age and color. This includes subgiants, young stars, and binaries. Subgiants were cut by removing stars with Gaia M_G absolute magnitude less than 4 check this, and stars with *both* $G_{BP} - G_{RP} < 1.5$ *and* kinematic age > 6 Gyr. Binaries were cut by fitting a 6th order polynomial.... etc. Here we define 'young stars' to mean stars that are too young to have converged onto the slow rotator sequence. These stars have rotation periods shorter than the bulk of the rotation period distribution. These young stars were removed by calculating their gyro-ages according to the Angus et al. (2019) empirical relation, and then excluding stars with gyro-ages younger than 0.7 Gyr. Hot stars...

- **Converting kinematic data to a grid.** Once applying these cuts, 20,000 kinematic stars remained. Given that fitting a GP to such a large dataset is computationally expensive, and given that 20,000 stars is far more than necessary to obtain a reasonably accurate gyrochronology model we opted to take averages of kinematic ages over a grid in rotation period and temperature. This provides the additional advantage of reducing the age uncertainties by the square root of the number of data points. This was beneficial because we did not include age uncertainties in our fit (so the smaller the age-uncertainties the better). For the clusters we can maybe get away with this, but the uncertainties on the kinematic are non-negligable (likely 1-2 Gyr Lu et al. 2021)). Figure **??** shows this grid in $P_{\rm rot}$-color space. Grid points were spaced apart by 0.5 dex in both $\log_{10}(P_{\rm rot})$ and Gaia color, $G_{BP} - G_{RP}$. The median age of all stars falling in a bin, centered on each grid point, was adopted as the age at that grid point. Only grid points with more than one data point in the corresponding bin were adopted. Figure **??** illustrates how this grid is still representative of the raw data, while reducing the number of data points in the fit, decreasing parameter uncertainties by $\sqrt{N}$, and providing uniform data coverage across the $P_{\rm rot}$-color plane.

- **Assigning rotation period uncertainties.** Although the rotation periods of stars in our sample often have reported uncertainties, these uncertainties alone are often not sufficient to describe the scatter in the data. Since we are using GP model, we require the data to be Gaussian-distributed, so instead of using the reported rotation period uncertainties we measured the uncertainties on the rotation periods empirically.

4.1. *Cross Validation*

In order to optimize the choices made above, and to quantify the overall age precision that can be expected from this model, we performed cross validation.

For each variable that needed to be optimized, we performed cross validation over a grid of values, and selected the value that resulted in the smallest root-mean-square (RMS) during cross validation. For example, for the uncertainties on the rotation periods of the kinematic data, we examined 10 uncertainty values between 1% and 10%. For each value, the GP model was re-trained and cross validation was performed. During cross validation we excluded 10 data points, selected at random from the combined cluster and kinematic calibration data set, and trained the model on the remaining data. We then
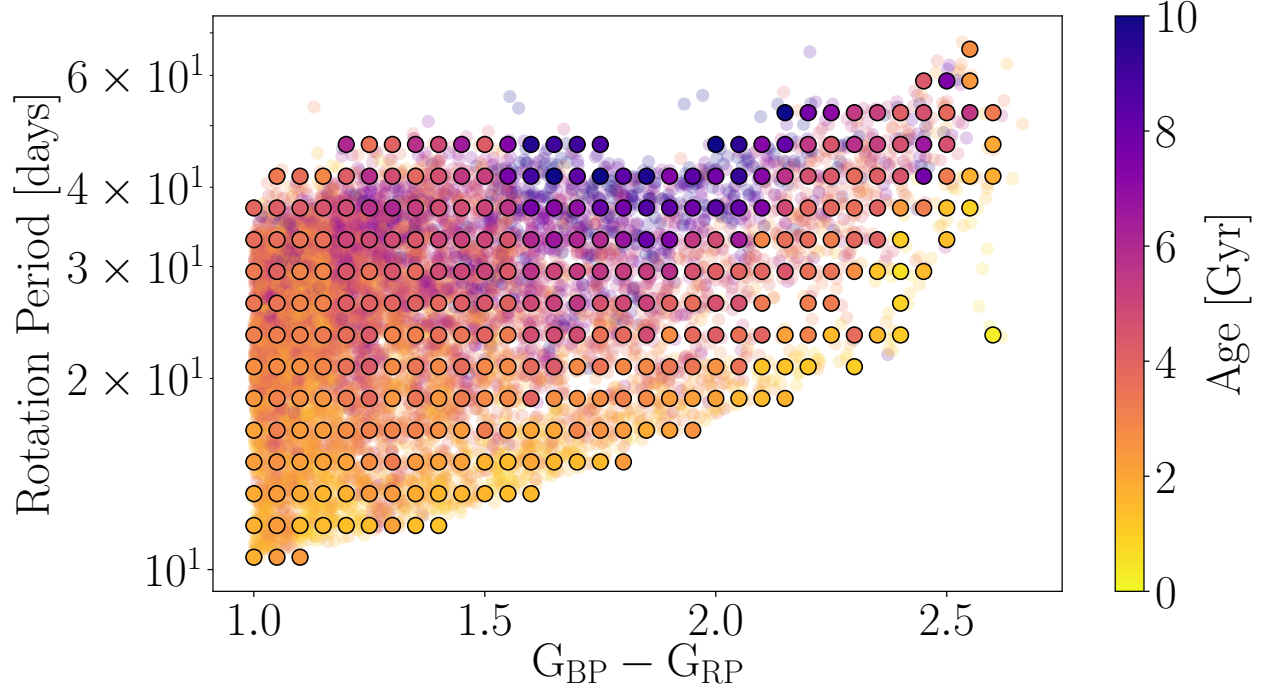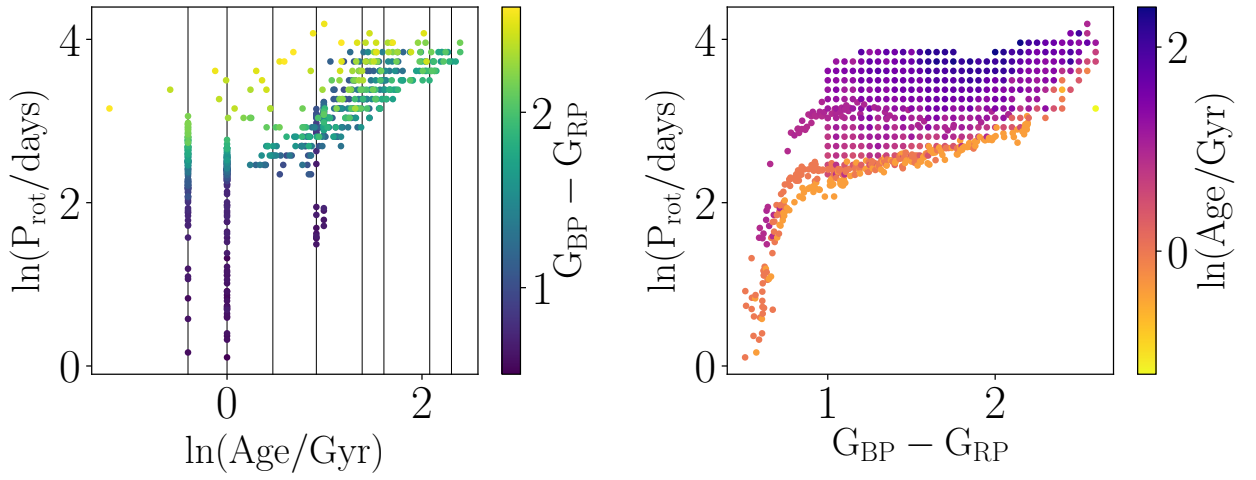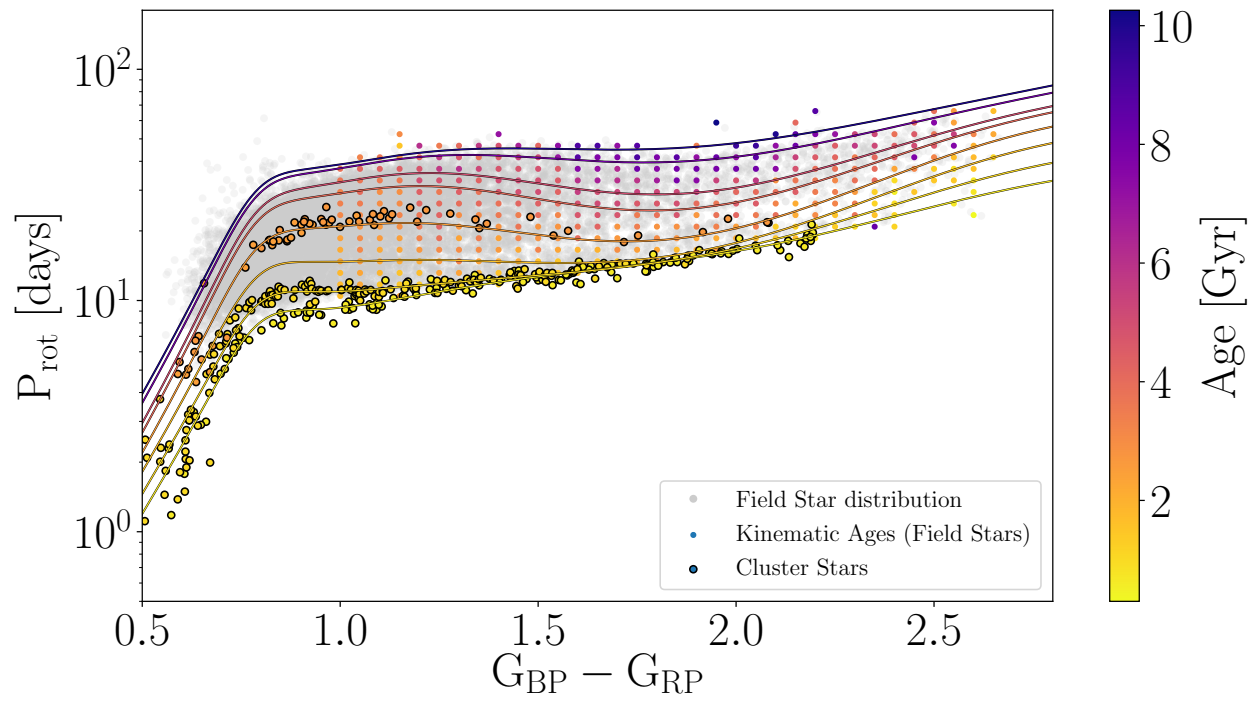
Figure 7.

Figure 8.

Figure 9.

5. RESULTS

6. DISCUSSION

7. CONCLUSION

REFERENCES

Agüeros, M. A., Bowsher, E. C., Bochanski, J. J., et al. 2018, ApJ, 862, 33, doi: 10.3847/1538-4357/aac6ed

Angus, R., Aigrain, S., & Foreman-Mackey *et al*, D. 2015, MNRAS, 450, 1787, doi: 10.1093/mnras/stv423

Angus, R., Morton, T. D., & Foreman-Mackey *et al*, D. 2019, AJ, 158, 173, doi: 10.3847/1538-3881/ab3c53

Angus, R., Beane, A., Price-Whelan, A. M., et al. 2020, AJ, 160, 90, doi: 10.3847/1538-3881/ab91b2

Astropy Collaboration, Robitaille, T. P., & Tollerud *et al*, E. J. 2013, A&A, 558, A33, doi: 10.1051/0004-6361/201322068

Aumer, M., Binney, J., & Schönrich, R. 2016, MNRAS, 462, 1697, doi: 10.1093/mnras/stw1639

Aumer, M., & Binney, J. J. 2009, MNRAS, 397, 1286, doi: 10.1111/j.1365-2966.2009.15053.x

Bailer-Jones, C. A. L. 2015, PASP, 127, 994, doi: 10.1086/683116

Bailer-Jones, C. A. L., Rybizki, J., & Fouesneau *et al*, M. 2018, AJ, 156, 58, doi: 10.3847/1538-3881/aacb21

Barnes, S. A. 2003, ApJ, 586, 464, doi: 10.1086/367639

—. 2007, ApJ, 669, 1167, doi: 10.1086/519295

—. 2010, ApJ, 722, 222, doi: 10.1088/0004-637X/722/1/222

Bird, J. C., Kazantzidis, S., & Weinberg *et al*, D. H. 2013, ApJ, 773, 43, doi: 10.1088/0004-637X/773/1/43

Brown, T. M., Latham, D. W., & Everett *et al*, M. E. 2011, AJ, 142, 112, doi: 10.1088/0004-6256/142/4/112

Casagrande, L., Schönrich, R., & Asplund *et al*, M. 2011, A&A, 530, A138, doi: 10.1051/0004-6361/201016276

Claytor, Z. R., van Saders, J. L., Santos, Â. R. G., et al. 2020, ApJ, 888, 43, doi: 10.3847/1538-4357/ab5c24

Cui, X.-Q., Zhao, Y.-H., & Chu *et al.*, Y.-Q. 2012, Research in Astronomy and Astrophysics, 12, 1197, doi: 10.1088/1674-4527/12/9/003

Curtis, J. L., Agüeros, M. A., & Douglas *et al*, S. 2019, arXiv e-prints. https://arxiv.org/abs/1905.06869

Curtis, J. L., Agüeros, M. A., Matt, S. P., et al. 2020, ApJ, 904, 140, doi: 10.3847/1538-4357/abbf58

Douglas, S. T., Agüeros, M. A., & Covey *et al*, K. R. 2017, ApJ, 842, 83, doi: 10.3847/1538-4357/aa6e52

Douglas, S. T., Curtis, J. L., & Agüeros *et al*, M. A. 2019, ApJ, 879, 100, doi: 10.3847/1538-4357/ab2468

Epstein, C. R., & Pinsonneault, M. H. 2014, ApJ, 780, 159, doi: 10.1088/0004-637X/780/2/159

Faherty, J. K., Burgasser, A. J., & Cruz *et al*, K. L. 2009, AJ, 137, 1, doi: 10.1088/0004-6256/137/1/1

Gaia Collaboration, Brown, A. G. A., & Vallenari *et al.*, A. 2018, A&A, 616, A1, doi: 10.1051/0004-6361/201833051

Gallet, F., & Bouvier, J. 2013, A&A, 556, A36, doi: 10.1051/0004-6361/201321302

Holmberg, J., Nordström, B., & Andersen, J. 2007, A&A, 475, 519, doi: 10.1051/0004-6361:20077221

—. 2009, A&A, 501, 941, doi: 10.1051/0004-6361/200811191

Irwin, J., & Bouvier, J. 2009, in IAU Symposium, Vol. 258, The Ages of Stars, ed. E. E. Mamajek, D. R. Soderblom, & R. F. G. Wyse, 363–374, doi: 10.1017/S1743921309032025

Kawaler, S. D. 1988, ApJ, 333, 236, doi: 10.1086/166740

Kiman, R., Schmidt, S. J., & Angus *et al*, R. 2019, AJ, 157, 231, doi: 10.3847/1538-3881/ab1753

Kraft, R. P. 1967, ApJ, 150, 551, doi: 10.1086/149359

Lu, Yuxi, Angus, R., et al. 2021, arXiv e-prints, arXiv:2102.01772. https://arxiv.org/abs/2102.01772

M. Green, G. 2018, The Journal of Open Source Software, 3, 695, doi: 10.21105/joss.00695

Mamajek, E. E., & Hillenbrand, L. A. 2008, ApJ, 687, 1264, doi: 10.1086/591785

Martig, M., Minchev, I., & Flynn, C. 2014, MNRAS, 443, 2452, doi: 10.1093/mnras/stu1322

McQuillan, A., Mazeh, T., & Aigrain, S. 2014, ApJS, 211, 24, doi: 10.1088/0067-0049/211/2/24

Meibom, S., Barnes, S. A., & Latham *et al*, D. W. 2011, ApJL, 733, L9, doi: 10.1088/2041-8205/733/1/L9

Meibom, S., Barnes, S. A., & Platais *et al*, I. 2015, Nature, 517, 589, doi: 10.1038/nature14118

Najita, J., Willman, B., & Finkbeiner *et al*, D. P. 2016, arXiv e-prints, arXiv:1610.01661. https://arxiv.org/abs/1610.01661

Nordström, B., Mayor, M., & Andersen *et al*, J. 2004, A&A, 418, 989, doi: 10.1051/0004-6361:20035959

Pinsonneault, M. H., Kawaler, S. D., & Sofia *et al*, S. 1989, ApJ, 338, 424, doi: 10.1086/167210

Price-Whelan, A. M., Sipőcz, B. M., & Günther *et al*, H. M. 2018, AJ, 156, 123, doi: 10.3847/1538-3881/aabc4f

Rebull, L. M., Stauffer, J. R., Cody, A. M., et al. 2018, AJ, 155, 196, doi: 10.3847/1538-3881/aab605

Rebull, L. M., Stauffer, J. R., & Hillenbrand *et al*, L. A. 2017, ApJ, 839, 92, doi: 10.3847/1538-4357/aa6aa4

Santos, A. R. G., García, R. A., & Mathur *et al*, S. 2019, ApJS, 244, 21, doi: 10.3847/1538-4365/ab3b56

Schatzman, E. 1962, Annales d'Astrophysique, 25, 18

Sellwood, J. A. 2014, Reviews of Modern Physics, 86, 1, doi: 10.1103/RevModPhys.86.1

Skumanich, A. 1972, ApJ, 171, 565, doi: 10.1086/151310

Soderblom, D. R. 2010, ARA&A, 48, 581, doi: 10.1146/annurev-astro-081309-130806

Spada, F., & Lanzafame, A. C. 2019, arXiv e-prints, arXiv:1908.00345. https://arxiv.org/abs/1908.00345

Stark, A. A., & Brand, J. 1989, ApJ, 339, 763,
doi: 10.1086/167334

Stark, A. A., & Lee, Y. 2005, ApJL, 619, L159,
doi: 10.1086/427936

Strömberg, G. 1946, ApJ, 104, 12, doi: 10.1086/144830

Ting, Y.-S., & Rix, H.-W. 2019, ApJ, 878, 21,
doi: 10.3847/1538-4357/ab1ea5

van Saders, J. L., Ceillier, T., & Metcalfe *et al*, T. S. 2016,
Nature, 529, 181, doi: 10.1038/nature16168

van Saders, J. L., Pinsonneault, M. H., & Barbieri, M.
2018, ArXiv e-prints.   https://arxiv.org/abs/1803.04971

Weber, E. J., & Davis, Jr., L. 1967, ApJ, 148, 217,
doi: 10.1086/149138

West, A. A., Bochanski, J. J., & Hawley *et al*, S. L. 2006,
AJ, 132, 2507, doi: 10.1086/508652

West, A. A., Hawley, S. L., & Bochanski *et al*, J. J. 2008,
AJ, 135, 785, doi: 10.1088/0004-6256/135/3/785

West, A. A., Hawley, S. L., & Walkowicz *et al*, L. M. 2004,
AJ, 128, 426, doi: 10.1086/421364

Wielen, R. 1977, A&A, 60, 263

Xiang, M., Ting, Y.-S., & Rix *et al.*, H.-W. 2019, ApJS,
245, 34, doi: 10.3847/1538-4365/ab5364

Yu, J., & Liu, C. 2018, MNRAS, 475, 1093,
doi: 10.1093/mnras/stx3204